



Upper bounds on the slump length in plug cementing of near-horizontal wells

I.A. Frigaard^{a,*}, G.A. Ngwa^b

^a Department of Mathematics and Department of Mechanical Engineering, University of British Columbia, 1984 Mathematics Road, Vancouver, BC, Canada V6T 1Z2

^b Department of Mathematics, University of Buea, P.O. Box 63, Buea, South West Province, Cameroon

Received 22 September 2003; received in revised form 21 January 2004

Abstract

When a near-horizontal well is sealed by means of a cement plug, a slow buoyancy-driven slumping flow can result along the axis of the well. The heavy plug slumps downwards along the bottom of the well, displacing the lighter wellbore fluids towards the top. Thus, a lower tail can slump down from the plug, towards the bottom of the well, while an upper tail can slump upwards, towards the top of the well. We derive a bound for the maximal length which the cement may slump, in each tail, before the motion is arrested by the yield stress of the cement slurry. We also predict the profile of the interface between fluids when the slumping motion stops. Our initial analysis is carried out for the geometrically simpler situation of a flow between parallel plates. Later we generalise our approach to flows in a pipe geometry, divided by a stratified interface.

© 2004 Published by Elsevier B.V.

Keywords: Cement plugs; Horizontal wells; Visco-plastic fluids; Yield limits

1. Introduction

The plug cementing process involves placing a volume \hat{V}_{plug} of cement into an oil well that is already full of another fluid. The aim of the cement plug is to form an impermeable hydraulic seal and a hard mechanical barrier. Details of the basic process can be found in either of the texts [1,2]. In the 1990s there was a significant increase in the number of wells drilled that were near-horizontal. It is the placing of cement plugs in such wells that we address in this paper.

A wellbore is an approximately cylindrical tube and horizontal well sections typically have diameter, $\hat{D} \leq 0.3$ m (often \hat{D} is in the range 0.1–0.15 m, for near-horizontal sections since these are in the production zone towards the end of the well). Cement plug lengths are typically in the range 50–100 m. The cement slurry is placed rapidly by pumping through a smaller diameter tube, which is then withdrawn. We consider the process in the minutes after the plug has been placed, but before the cement begins to harden.

A typical cement slurry density is around 1900 kg/m³, and the surrounding fluids (drilling mud, viscous pill, spacer fluid, or simply residual reservoir fluids: oil/water), have a much lower density: 1000–1700 kg/m³. Because of the density difference, there will be a natural tendency for the heavier fluid to move towards the bottom of the well, displacing lighter fluids upwards. At the lower end of the plug, a tail is likely to develop that propagates downwards in the well. Similarly, at the upper end of the plug, a tail will slump upwards along the bottom, see Fig. 1.

The driving force for the slow slumping motion is the density difference combined with the slope of the interface between fluids. If the fluids were Newtonian, the final equilibrium position would be that the fluids sit stratified at the bottom of the well, with the lighter fluids on top, i.e. purely viscous stresses cannot resist motion. If, however, the fluids have a yield stress and the inclination to the horizontal direction is sufficiently small, one would expect that the interface stretches axially to such an extent that the buoyant driving force cannot overcome the yield stresses of the fluids. Thus, eventually the fluids become static and, if sufficient cement was pumped, one has an intact cement plug of length \hat{L}_{plug} filling the well. It is this problem that we consider in this

* Corresponding author. Fax: +1-604-822-6074.

E-mail address: frigaard@math.ubc.ca (I.A. Frigaard).

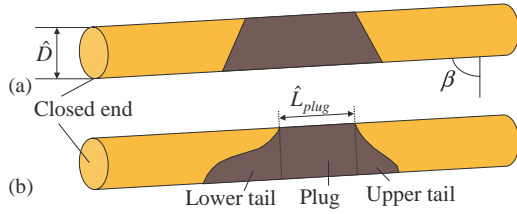


Fig. 1. Schematic diagram of cement plug geometry: (a) post-placement; (b) after the plug has slumped to its static length.

62 paper. Relevant questions are: what are the yield stresses re- 86
 63 quired to arrest the slow slumping motion of a cement plug 87
 64 down-hole, how far will the slumping flow propagate, what 88
 65 volume \hat{V}_{plug} must be pumped to ensure an intact plug of 89
 66 length \hat{L}_{plug} ? 90

67 The placing of cement plugs in non-horizontal sections 92
 68 has received some attention in the technical cementing litera- 93
 69 ture over the years, e.g. [3–8], and also the fluid mechan- 94
 70 ics literature, [9–13]. Most analyses have focused on the 95
 71 post-placement phase of plug cementing and on understand- 96
 72 ing the evolution of a slumping flow. That slow axial slump- 97
 73 ing flows do occur for realistic fluid physical properties can 98
 74 be seen in the experimental work of [5,8]. The slumping 99
 75 flow is approximately uni-directional, along the axis of the 100
 76 well, at least far from the advancing fronts. Analytical ap- 101
 77 proaches date back to the work of [3]. In such approaches 102
 78 the fluids are usually modelled as inelastic visco-plastic flu- 103
 79 ids (Bingham fluids or Herschel–Bulkley fluids). 104

80 For an infinitely long cylindrical duct containing two yield 105
 81 stress fluids, it can be shown via dimensional analysis that 106
 82 any criteria that defines when the flow is stationary should 107
 83 depend only on the inclination of the well, β (see Fig. 1), 108
 84 and on the following two dimensionless yield stresses: 109

$$85 \tau_{c,Y}^* \equiv \frac{\hat{\tau}_{c,Y}}{[\hat{\rho}_c - \hat{\rho}_m]\hat{g}\hat{D}}, \quad \tau_{m,Y}^* \equiv \frac{\hat{\tau}_{m,Y}}{[\hat{\rho}_c - \hat{\rho}_m]\hat{g}\hat{D}}. \quad (1)$$

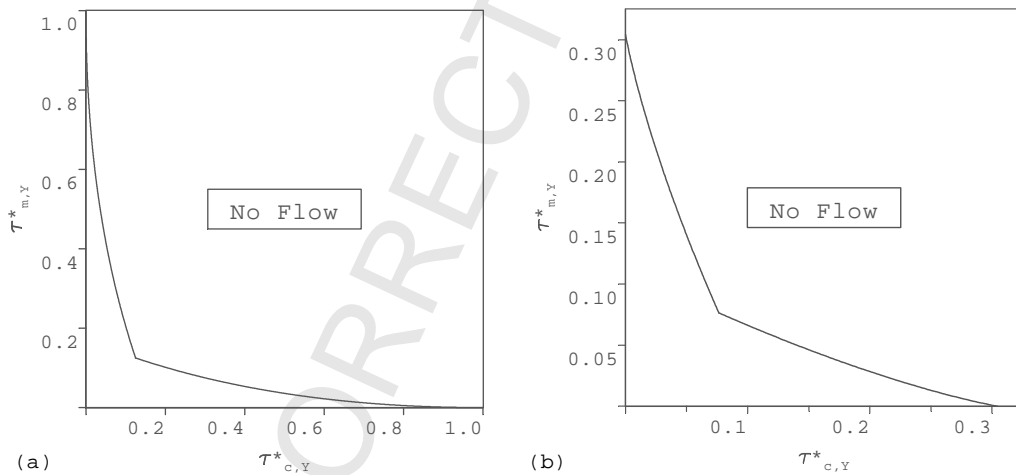


Fig. 2. Conditions on $\tau_{c,Y}^*$ and $\tau_{m,Y}^*$ for which the axial velocity, $w = 0$: (a) slot flow (between parallel plates) with zero net flow, from [9]; (b) flow in a circular cylinder with planar interface and zero net flow, from [13].

In (1), the two fluids are distinguished by the subscripts c 86
 and m (c denoting the heavier fluid), \hat{g} is the gravitational 87
 acceleration, the yield stresses are denoted $\hat{\tau}_{c,Y}$ and $\hat{\tau}_{m,Y}$, 88
 and the densities are $\hat{\rho}_c$ and $\hat{\rho}_m$ (in this paper dimensional 89
 quantities are denoted by a hat symbol, $\hat{\cdot}$, and dimensionless 90
 variables without). 91

At fixed inclination, as the two dimensionless yield 92
 stresses in (1) are increased beyond a critical curve, the 93
 flow stops. Examples of these zero-flow criteria have been 94
 derived in [9,12,13], for different geometries and interface 95
 configurations. For example, in an infinite horizontal well 96
 containing two yield stress fluids, if the interface between 97
 the fluids is vertical then there is no motion provided that: 98

$$\tau_{c,Y}^* + \tau_{m,Y}^* \geq \frac{1}{4}. \quad (2)$$

In an infinite two-dimensional vertical cavity (e.g. between 100
 parallel plates separated a distance \hat{D}), with the interface 101
 also vertical, there is no motion if $|(\tau_{c,Y}^*, \tau_{m,Y}^*)|$ exceeds the 102
 curve in Fig. 2a; see [9]. For a vertical well with a vertical 103
 planar interface separating the two fluids, the yield stresses, 104
 $|(\tau_{c,Y}^*, \tau_{m,Y}^*)|$, must exceed the curve in Fig. 2b in order for 105
 the axial velocity to be identically zero; see [13]. Note that 106
 these results are symmetric with respect to the yield stresses 107
 (i.e. about the line $\tau_{c,Y}^* = \tau_{m,Y}^*$), and that stationary flows 108
 are achieved for minimal $|(\tau_{c,Y}^*, \tau_{m,Y}^*)|$, when $\tau_{c,Y}^* = \tau_{m,Y}^*$. 109
 The symmetry is because the flow is buoyancy driven and 110
 the density difference acts equally to push light fluids up- 111
 wards and heavy fluids downwards, i.e. there is no asymme- 112
 try between the fluids. We shall return to these results later. 113

It will be noted from (2) and Fig. 2, that $|(\tau_{c,Y}^*, \tau_{m,Y}^*)| \sim$ 114
 $O(1)$ in order to stop the above flows, in all of which the 115
 interface is parallel to the direction of gravity. For typical 116
 parameters in plug cementing, $[\hat{\rho}_c - \hat{\rho}_m]\hat{g}\hat{D} \sim O(10^2)$ Pa, 117
 which implies that large yield stresses are needed when the 118
 interface is vertical. Fluids with large yield stresses are, 119
 however, impractical for pumping into long near-horizontal

wells.¹ Consequently, it is preferable to allow the fluids to slump, so that the interfaces become closer to horizontal and much smaller yield stresses can stop the flow. It is this question that we address in this paper, i.e. assuming that the yield stresses are insufficient to prevent motion, according to a criteria such as (2), and that slumping occurs, how far will the slumping flow propagate before buoyancy effects are small enough for the flow to stop.

The approach that we take in this paper is to model both the cement plug and surrounding fluids as Bingham fluids. We use the classical scaling arguments of thin-film/lubrication theory, similar to those used in [9,10], to reduce the model complexity. For the lubrication model, we then consider the minimal surface inclination required in order for the fluids to flow. Integrating this expression we derive an expression for the stopping surface, and hence the slump lengths.

Although there are similarities between this paper and [9–11], there is a key mathematical difference in the motion of the interface, which is common to other thin-film/lubrication flows. In a near axial flow in a well that is far from horizontal, the inclination of the well is dominant over the inclination of the interface. The latter is therefore usually neglected in deriving the leading order axial momentum balance(s) and the resulting equations for the interface motion are hyperbolic, see e.g. [11]. If on the other hand, the inclination of the well is comparable with the inclination of the interface (which is the case in a near-horizontal well), then the interface inclination cannot be ignored. The resulting equations for the interface motion are parabolic.

There have been a large number of works in which thin-film/lubrication theory has been used to model the flow of a single visco-plastic fluid along a sloping surface. For example, lava flows have been studied extensively in [14–18]. Flows of mud have been studied in [19–26]. Similar flows, on the outside of large cylinders are treated in [27,28], and free-surface lubrication flows of visco-plastics have been studied in more generality in [29,30]. With these papers, a mix of analytical, numerical and experimental methods have been used. Our work differs from these above in that we consider multiple fluids. Secondly, we impose the constraint that there is zero net flow along the well (since the lower

end of the wellbore is closed). Both features complicate the problem considerably, since it is not possible to compute separately the flow in each fluid layer and the conditions for the flow to stop (for a single fluid thin film, this is simply related to the height), are consequently harder to derive.

In this paper we compute a limiting interface profile at which the flow will stop, for the upper and lower slump tails. We compute the interface profile directly as a steady-state problem. Various computations of this type have been made for the single fluid lubrication problems listed above, although it is equally common to compute the initial value problem for the interface, see e.g. [26]. We comment that various attempts have also been made to interpret rheological parameters from the shape of the final static surface in such flows, e.g. [21,31].

An outline of the paper is as follows. In Section 2 we introduce the scaled model for slumping flows in an oil well, and simplify to a lubrication model. Section 3 considers the slumping flow in a slot. We derive sufficient conditions on the interface for a static flow and derive expressions for both the shape of the interface between the two fluids and the slump length. Results are computed that show variation with the key parameters. Section 4 generalises this approach to the more physically relevant problem of stratified exchange flows in a circular pipe, again providing expressions for the interface shape and slump length. The article finishes with a short discussion. The relationship between the different approaches in Sections 3 and 4 is explained in Appendix A.

2. Slow slumping motion of a cement plug in a near-horizontal well

We consider a long duct (either a circular oil well, or for simplification a slot), that is approximately horizontal. The duct is sealed at one end, assumed far away from the domain of interest, and is filled with two immiscible and incompressible fluids: a heavy cement slurry and a lighter mud ($\hat{\rho}_c > \hat{\rho}_m$). In the scenario we consider, the cement has been placed in the duct, with volumes of mud both above and below it, see Fig. 1a. A slow slumping flow has initiated, with the cement slurry slumping toward the base of the duct, displacing the mud towards the roof of the duct. Both fluids are considered visco-plastic, i.e. they possess a finite yield stress. However, we assume that

$$0 < \tau_{c,Y}^* + \tau_{m,Y}^* \ll 1, \quad (3)$$

so that (2) and similar criteria are not satisfied and the slump flow occurs. We assume the total cement volume is sufficient that the motion stops with an *intact length*, \hat{L}_{plug} , of cement that completely fills the duct section, see Fig. 1b. This enables us to consider the motion of the upper and lower tails separately. The duct height is denoted \hat{D} .

The underlying model is similar to that considered previously, in [9–11,13]. The pressure and velocity are denoted $\hat{p}(\hat{x}, \hat{t})$ and $\hat{u}(\hat{x}, \hat{t})$, respectively. The stress and deviatoric

¹ In most wellbore pumping operations one attempts to keep the hydraulic pressure in the well between the pore pressure and the fracture pressure: in the *pore-fracture envelope*. The fracture pressure is the hydraulic pressure at which the formation fractures and the pore pressure is the pressure of the fluids in the formation. To exceed the fracture pressure results in fracturing the rock formation and to fall below the pore pressure results in a fluid influx, both of which are generally undesirable. Maintaining this balance is referred to as maintaining *primary control* of the well, which is typically achieved by controlling both static and frictional pressures. Both fracture pressure and pore pressure generally increase with depth. However, in a near-horizontal section, the longer the section the higher the frictional pressure becomes, whereas the static, pore and fracture pressures all remain constant.

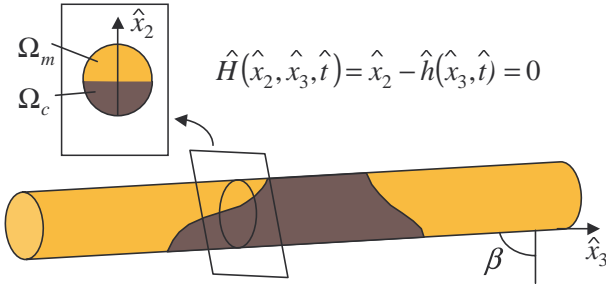


Fig. 3. Geometry and coordinates of the lubrication model.

Constitutive laws for the Bingham fluids are

$$\hat{\gamma}(\hat{\mathbf{u}}) = 0 \Leftrightarrow \hat{\tau}_k(\hat{\mathbf{u}}) \leq \hat{\tau}_{k,Y}, \quad \hat{\mathbf{x}} \in V_k, \quad (9)$$

$$\hat{\tau}_{k,ij}(\hat{\mathbf{u}}) = \left[\hat{\mu}_k + \frac{\hat{\tau}_{k,Y}}{\hat{\gamma}(\hat{\mathbf{u}})} \right] \hat{\gamma}_{ij}(\hat{\mathbf{u}}) \Leftrightarrow \hat{\tau}_k(\hat{\mathbf{u}}) > \hat{\tau}_{k,Y}, \quad \hat{\mathbf{x}} \in V_k. \quad (10)$$

The constants $\hat{\mu}_k : k = c, m$, are the plastic viscosity for each fluid, assumed to be strictly positive.

2.1. Reduced model

We consider the coordinate $\hat{z} = \hat{x}_3$ to be aligned with the duct axis, with $(\hat{x}, \hat{y}) = (\hat{x}_1, \hat{x}_2)$ in the cross-section of the duct; see Fig. 3. The cross-section of the duct is denoted Ω and the cross-sectional areas occupied by the cement and the mud are denoted as Ω_c and Ω_m . Clearly Ω_c and Ω_m will vary with length along the duct. To reduce the model, we will adopt a typical thin-film/lubrication for our variables. The small parameter δ , which will serve as the aspect ratio, is defined by:

$$\delta = \frac{\max\{\hat{\tau}_{c,Y}, \hat{\tau}_{m,Y}\}}{\Delta \hat{\rho} \hat{g} \hat{D}} \ll 1. \quad (11)$$

Our scaling is

$$x_1 = \frac{\hat{x}_1}{\hat{D}}, \quad x_2 = \frac{\hat{x}_2}{\hat{D}}, \quad x_3 = \delta \frac{\hat{x}_3}{\hat{D}}, \quad (12)$$

$$u_1(\mathbf{x}, t) = \frac{\hat{u}_1(\hat{\mathbf{x}}, \hat{t})}{\delta \hat{U}_0}, \quad u_2(\mathbf{x}, t) = \frac{\hat{u}_2(\hat{\mathbf{x}}, \hat{t})}{\delta \hat{U}_0}, \quad (13)$$

$$u_3(\mathbf{x}, t) = \frac{\hat{u}_3(\hat{\mathbf{x}}, \hat{t})}{\hat{U}_0}. \quad (13)$$

$$p(\mathbf{x}, t) = \frac{\hat{p}(\hat{\mathbf{x}}, \hat{t}) - \hat{p}_0}{\hat{\rho} \hat{g} \hat{D}}, \quad \tau_{k,ij} = \frac{\hat{\tau}_{k,ij}}{\Delta \hat{\rho} \hat{g} \hat{D} \delta}. \quad (14)$$

The velocity scale is defined by:

$$\hat{U}_0 = \frac{\delta \Delta \hat{\rho} \hat{g} \hat{D}^2}{\hat{\mu}_c}, \quad (15)$$

\hat{p}_0 is a reference pressure, the mean density and the density difference are defined by

$$\hat{\rho} = \frac{1}{2}[\hat{\rho}_c + \hat{\rho}_m], \quad \Delta \hat{\rho} = \hat{\rho}_c - \hat{\rho}_m. \quad (16)$$

Adopting this scaling and neglecting the inertial terms, we derive the following leading order equations:

$$\frac{\partial p}{\partial x_1} = 0, \quad \mathbf{x} \in \Omega_k, \quad (16)$$

$$\frac{\partial p}{\partial x_2} + \phi_k = 0, \quad \mathbf{x} \in \Omega_k, \quad (17)$$

$$\frac{1}{\phi} \left[\frac{\partial p}{\partial x_3} + \alpha \phi_k \right] = \frac{\partial \tau_{k,31}}{\partial x_1} + \frac{\partial \tau_{k,32}}{\partial x_2}, \quad \mathbf{x} \in \Omega_k, \quad (18)$$

stress tensors are denoted $\hat{\sigma}_{ij}$ and $\hat{\tau}_{k,ij}$, $k = c, m$, respectively. The equations of motion, valid within each fluid region, V_k , $k = c, m$, are

$$\hat{\rho}_k \frac{D\hat{\mathbf{u}}_i}{D\hat{t}} = -\frac{\partial \hat{p}}{\partial \hat{x}_i} + \frac{\partial}{\partial \hat{x}_j} \hat{\tau}_{k,ij} + \hat{g}_{k,i}, \quad (4)$$

$$\frac{\partial \hat{u}_j}{\partial \hat{x}_j} = 0, \quad (5)$$

with coordinates as indicated in Fig. 3. The gravitational body force \hat{g}_k , in fluid k , is defined by

$$\hat{g}_k = (0, -\hat{\rho}_k \hat{g} \sin \beta, -\hat{\rho}_k \hat{g} \cos \beta), \quad (6)$$

where $\cos \beta \ll 1$, and the material derivative is

$$\frac{D}{D\hat{t}} \equiv \frac{\partial}{\partial \hat{t}} + \hat{u}_j \frac{\partial}{\partial \hat{x}_j}.$$

No slip conditions are satisfied on the walls of the duct, stress and velocity vectors are continuous across the interface, and the fluid is quiescent sufficiently far from the domain of interest, around the cement stage. The interface between the two volumes is advected via a kinematic condition. Surface tension is assumed insignificant (or equivalently we may consider the fluids miscible, but over a sufficiently short timescale).

The rheologies assumed are those of Bingham fluids. The yield stresses play the critical role in our flow and the Bingham model is the simplest yield stress fluid. The actual yielded flow behaviour (where more non-linear models may be more appropriate), is of secondary importance. The rate of strain and deviatoric stress second invariants, $\hat{\gamma}(\hat{\mathbf{u}})$ and $\hat{\tau}_k(\hat{\mathbf{u}})$, respectively, are defined by:

$$\hat{\gamma}(\hat{\mathbf{u}}) = \left[\frac{1}{2} \sum_{i,j=1}^3 [\hat{\gamma}_{ij}(\hat{\mathbf{u}})]^2 \right]^{1/2}, \quad (7)$$

$$\hat{\tau}_k(\hat{\mathbf{u}}) = \left[\frac{1}{2} \sum_{i,j=1}^3 [\hat{\tau}_{k,ij}(\hat{\mathbf{u}})]^2 \right]^{1/2}, \quad (7)$$

where

$$\hat{\gamma}_{ij}(\hat{\mathbf{u}}) = \frac{\partial \hat{u}_i}{\partial \hat{x}_j} + \frac{\partial \hat{u}_j}{\partial \hat{x}_i}. \quad (8)$$

$$0 = \frac{\partial u_j}{\partial x_j}, \quad (19)$$

where

$$\phi_k = \frac{\hat{\rho}_k}{\hat{\rho}}, \quad \phi = \frac{\Delta \hat{\rho}}{\hat{\rho}} \quad (20)$$

and note that $\phi_c + \phi_m = 2$ and $\phi_c - \phi_m = \phi$. The parameter α is defined by

$$\alpha = \frac{\cos \beta}{\delta}. \quad (21)$$

We later refer to α as the inclination. What we mean by the well being *near-horizontal* is that $\alpha = O(1)$, and we shall define a precise upper bound on α for our flows. Eqs. (16)–(19) do not depend explicitly on time t , but do so implicitly through the interface position. The interface $H = 0$ is simply advected:

$$\frac{DH}{Dt} = 0. \quad (22)$$

2.1.1. Constitutive laws

The leading order approximations to the full constitutive laws in fluid k are

$$\tau_k \leq \tau_{k,Y} \Leftrightarrow |\nabla u_3| = 0, \quad (23)$$

$$\tau_k > \tau_{k,Y} \Leftrightarrow \begin{cases} \tau_{k,31} = \left[\mu_k + \frac{\tau_{k,Y}}{|\nabla u_3|} \right] \frac{\partial u_3}{\partial x_1}, \\ \tau_{k,32} = \left[\mu_k + \frac{\tau_{k,Y}}{|\nabla u_3|} \right] \frac{\partial u_3}{\partial x_2}, \end{cases} \quad (24)$$

where

$$\tau_{k,31}^2 + \tau_{k,32}^2 = \tau_k^2, \quad |\nabla u_3|^2 = \left(\frac{\partial u_3}{\partial x_1} \right)^2 + \left(\frac{\partial u_3}{\partial x_2} \right)^2.$$

Although four parameters appear above, there are only two independent dimensionless rheological parameters. These are the viscosity ratio and the minimum yield stress:

$$m = \frac{\hat{\mu}_m}{\hat{\mu}_c}, \quad \tau_{\min,Y} = \frac{\min\{\hat{\tau}_{c,Y}, \hat{\tau}_{m,Y}\}}{\Delta \hat{\rho} \hat{g} \hat{D} \delta}, \quad k = c, m. \quad (25)$$

Note, we have defined the velocity scaling using the cement plastic viscosity and used the maximum yield stress in defining δ . Thus we have $\mu_c = 1$, $\mu_m = m$, and either of $\tau_{c,Y} = \tau_{\min,Y}$, $\tau_{m,Y} = 1$, or $\tau_{c,Y} = 1$, $\tau_{m,Y} = \tau_{\min,Y}$.

2.1.2. Simplified momentum balance

Hereafter, we shall assume a single-valued stratified interface dividing mud and cement:

$$H = x_2 - h(x_3, t) = 0. \quad (26)$$

From (16) it follows that $p = p(x_2, x_3, t)$, and integrating (17):

$$p(x_2, x_3, t) = \begin{cases} p(0, x_3, t) - \phi_c x_2, & x_2 < h(x_3, t), \\ p(0, x_3, t) - \phi h(x_3, t) - \phi_m x_2, & x_2 > h(x_3, t). \end{cases} \quad (27)$$

We now define a modified pressure $P(x_3, t)$ by:

$$P(x_3, t) = h(x_3, t) - \frac{p(0, x_3, t) + \alpha \phi_m x_3}{\phi}. \quad (28)$$

Substituting into (18) gives:

$$b - f = \frac{\partial \tau_{c,31}}{\partial x_1} + \frac{\partial \tau_{c,32}}{\partial x_2}, \quad x_2 < h(x_3, t), \quad (29)$$

$$-f = \frac{\partial \tau_{m,31}}{\partial x_1} + \frac{\partial \tau_{m,32}}{\partial x_2}, \quad x_2 > h(x_3, t), \quad (30)$$

where

$$f = \frac{\partial P}{\partial x_3}, \quad b = \alpha + \frac{\partial h}{\partial x_3}. \quad (31)$$

Here f will be referred to as the modified pressure gradient and b as the buoyancy parameter.

Eqs. (29) and (30) are similar to the system considered in [9,11,13], and for a fixed interface gradient are analogous. These equations are integrated to give the axial velocity u_3 , which can then be combined with (19) and (22) to give a conservation equation for the interface motion. However, although the problem for u_3 on each cross-section is similar to [9,11,13] (apart from scaling), the transient problem for the interface motion is different, due to dependency of b on the gradient of h .

3. Slumping flow in a slot

The simplest version of our model problem occurs when the duct is considered to be a two-dimensional slot, i.e. of infinite extent and uniform in the x_1 -direction. We drop the subscripts for simplicity. The static problem at each $z = x_3$, is to find the axial velocity $w(y)$ ($y = x_2$), satisfying:

$$b - f = \frac{d}{dy} \tau_{c,zy}, \quad y < h(z, t), \quad (32)$$

$$-f = \frac{d}{dy} \tau_{m,zy}, \quad y > h(z, t), \quad (33)$$

where for $k = c, m$

$$|\tau_{k,zy}| \leq \tau_{k,Y} \Leftrightarrow |w'(y)| = 0, \quad (34)$$

$$|\tau_{k,zy}| > \tau_{k,Y} \Leftrightarrow \tau_{k,zy} = \left[\mu_k + \frac{\tau_{k,Y}}{|w'(y)|} \right] w'(y). \quad (35)$$

Boundary conditions are $w(0) = w(1) = 0$, and at the interface between cement and mud, both $w(y)$ and the shear

351 stresses are continuous. The final condition comes from the
 352 fact that the lower end of the duct is closed, and thus the net
 353 flow at any position z must equal zero:

$$354 \int_0^1 w(y) dy = 0. \quad (36)$$

355 For finite $b > 0$, the problem (32)–(36) is equivalent to that
 356 considered in [9], where $b = 1$. Many of the general qual-
 357 itative results from [10,13] are relevant. We summarise the
 358 main results. A solution (w, f) exists and is unique provided
 359 that $\|w\| \neq 0$, which may occur for a finite range of f . The
 360 parameter f will lie in the range $(0, b)$. The solution is con-
 361 tinuous with respect to the material properties (in appropri-
 362 ate norms). Various monotonicity results were also proven,
 363 with respect to the different material parameters.

364 In place of the kinematic equation for h , it is straightfor-
 365 ward to derive the following mass conservation equation:

$$366 \frac{\partial h}{\partial t} + \frac{\partial}{\partial z} Q_c = 0, \quad (37)$$

367 where, as is common in thin-film flows, we find that

$$368 w(y, z, t) = w(y, h(z, t), h_z(z, t)), \quad (38)$$

369 and where

$$370 Q_c = \int_{\Omega_c} w(y, z, t) dy = Q_c(h, h_z). \quad (39)$$

371 In the case that $b = \text{constant}$, we have simply $w =$
 372 $w(y, h(z, t))$ and hence $Q_c = Q_c(h)$. In that case, Eq. (37)
 373 is a hyperbolic equation for h . This problem is considered
 374 in detail in [11]. Here, b is not constant and it is clear that
 375 (37) is a second-order partial differential equation for h .

376 3.1. Static flow conditions and slump length in a slot

377 We focus here on the lower tail of the cement plug in
 378 Fig. 1, stating later the results for the upper tail. Taking the
 379 problem (29)–(36) and re-scaling the stresses and f with the
 380 buoyancy parameter b , we recover exactly the mathematical
 381 problem considered in [9]. We denote the re-scaled yield
 382 stresses $(\tau_{c,Y}^*, \tau_{m,Y}^*)$ by:

$$383 \tau_{k,Y}^* = \frac{\tau_{k,Y}}{b}, \quad k = c, m, \quad \tau_{\min,Y}^* = \frac{\tau_{\min,Y}}{b}. \quad (40)$$

384 In [9] it is shown that whether or not there exists a non-trivial
 385 solution ($w \neq 0$) will depend on the height of the interface,
 386 h , and the two yield stresses $(\tau_{c,Y}^*, \tau_{m,Y}^*)$. A necessary and
 387 sufficient condition to ensure that $w = 0$, for fixed h , is that:

$$388 1 \leq \frac{\tau_{c,Y}^*}{h} + \frac{\tau_{m,Y}^*}{1-h} + \tau_{\min,Y}^* \left(\frac{1}{h} + \frac{1}{1-h} \right). \quad (41)$$

389 If we consider the maximum of the right-hand side of (41),
 390 over all h , and evaluate when this maximum is equal to 1, we
 391 derive the marginal curve, separating trivial and non-trivial
 392 solutions in the $(\tau_{c,Y}^*, \tau_{m,Y}^*)$ plane. This is given by:

$$393 1 + (\tau_{c,Y}^* - \tau_{m,Y}^*)^2 - 2(\tau_{c,Y}^* + \tau_{m,Y}^* + 2\tau_{\min,Y}^*) = 0 \quad (42)$$

for $|\tau_{c,Y}^* - \tau_{m,Y}^*| < 1$. This curve is plotted in Fig. 2a (note
 that the definitions of $(\tau_{c,Y}^*, \tau_{m,Y}^*)$ in the introduction and
 here are different). The derivation of (41) in [9] is based on
 physical arguments; later we will give a more mathematical
 derivation.

Multiplying through by b , we can rewrite (41) at each z ,
 as

$$\alpha + \frac{\partial h}{\partial z} \leq \frac{\tau_{c,Y}}{h} + \frac{\tau_{m,Y}}{1-h} + \tau_{\min,Y} \left(\frac{1}{h} + \frac{1}{1-h} \right). \quad (43)$$

It is evident that (43) leads to an upper bound on the length of
 the lower tail. Let us suppose that the cement plug is initially
 placed as shown schematically in Fig. 1a. The gradients in
 h are initially very large and hence we suppose that the
 slumping motion that we have discussed is initiated. As the
 cement plug spreads along the well into the lower tail, the
 gradient of h will decrease. Consider first the case that $\alpha =$
 0, i.e. a horizontal well. It is evident that, at each h , the
 interface will spread out until it attains a minimal critical
 gradient, beyond which (43) is violated. At that point, since
 $w = 0$, we also have $Q_c = 0$ and from (37), we see that the
 interface motion halts.

For $\alpha \neq 0$, the same type of behaviour is expected, but
 only if α is not so large as to drive the flow by itself. The
 condition for this to occur can be found from (42). Since the
 maximal yield stress is equal to 1, we have that

$$\alpha \leq 2(\tau_{c,Y} + \tau_{m,Y} + 2\tau_{\min,Y}) - (\tau_{c,Y} - \tau_{m,Y})^2 \\ = 1 + 8\tau_{\min,Y} - \tau_{\min,Y}^2. \quad (44)$$

For given $\tau_{\min,Y}$, condition (44) defines the limiting incli-
 nation α above which the flow will propagate. We see that
 a sufficient bound on α is that $\alpha \leq 1$.

The minimal gradient of $h(z)$ obviously corresponds to
 a maximal gradient of $z(h)$ which limits the slump length.
 Assuming (44), we find the maximal length $z_{l,\max}(h)$, that
 the lower tail is able to slump before the surface gradient is
 unable to drive the flow is given by integrating:

$$\frac{d}{dh} z_{l,\max} = \frac{1}{(\tau_{c,Y}/h) + (\tau_{m,Y}/(1-h)) + \tau_{\min,Y}((1/h) + (1/(1-h))) - \alpha}. \quad (45)$$

The maximal length which the lower tail can slump, L_{lower} ,
 is given by integrating (45) from $h = 0$ to 1, i.e.

$$L_{\text{lower}} = \int_0^1 \frac{1}{(\tau_{c,Y}/h) + (\tau_{m,Y}/(1-h)) + \tau_{\min,Y}((1/h) + (1/(1-h))) - \alpha} dh, \quad (46)$$

and the total cement volume in the tail (per unit length in
 the x -direction), is:

$$V_{\text{lower}} = L_{\text{lower}} - \int_0^1 z_{l,\max}(h) dh. \quad (47)$$

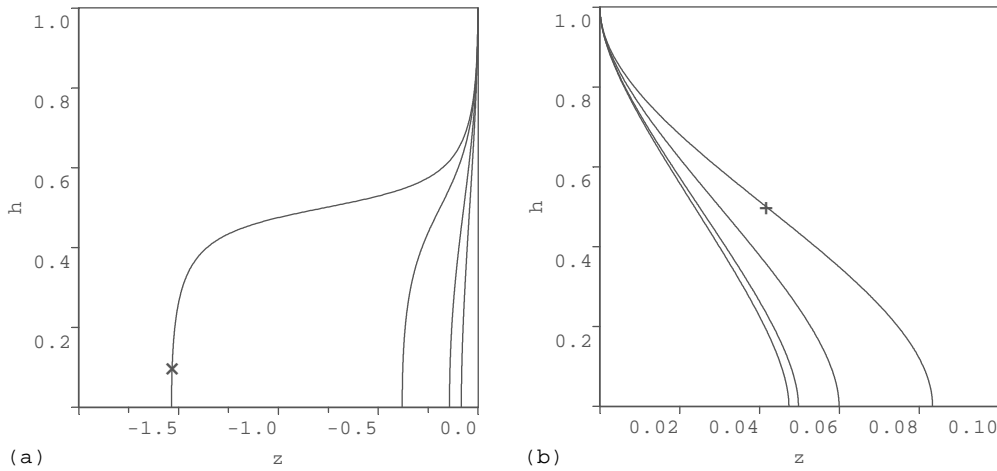


Fig. 4. Variation of upper and lower slump tail shape with increasing inclination, $\alpha = 0, 4, 7, 7.9$; $\alpha_{crit} = 8$: fixed parameters, $\tau_{c,Y} = \tau_{m,Y} = 1$: (a) lower slump tail increases with α , the curve $\alpha = 7.9$ is marked with a \times ; (b) upper slump tail decreases with α , the curve $\alpha = 0$ is marked with a $+$.

439 An identical analysis may be carried out for the upper tail,
440 giving the following:

$$\frac{d}{dh} z_{u,max} = \frac{1}{(\tau_{c,Y}/h) + (\tau_{m,Y}/(1-h)) + \tau_{min,Y}((1/h) + (1/(1-h))) + \alpha}, \quad (48)$$

$$L_{upper} = \int_0^1 \frac{1}{(\tau_{c,Y}/h) + (\tau_{m,Y}/(1-h)) + \tau_{min,Y}((1/h) + (1/(1-h))) + \alpha} dh, \quad (49)$$

$$V_{upper} = L_{upper} - \int_0^1 z_{u,max}(h) dh. \quad (50)$$

446 For the upper tail, it is clear that no bound on α need be
447 assumed in order to prevent the plug from flowing uphill.
448 However, condition (44) is still necessary in the context of
449 the plug cementing problem. This is because if (44) is not

satisfied the lower tail will not stop and the final position of
the entire cement plug will be at the bottom of the well.

3.2. Results

We first illustrate the effects of inclination on the slumping
flow. Fixing $\tau_{c,Y} = \tau_{m,Y} = 1$ we increase the inclination
from $\alpha = 0$, up to close to the critical value, $\alpha_{crit} = 8$, at
which the slumping does not stop, see Fig. 4. We can see that
the upper tail decreases as the lower tail extends. It is only
close to the critical value of α that the lower slump length
becomes $O(1)$ and then increases to infinity. Fig. 5 plots
the variation of slump lengths and volumes with inclination,
for the same parameters as in Fig. 4. Since the geometry is
rectangular, the two measures are quite similar.

In Fig. 6 we investigate how the shape of the slump tails
change with fluid rheology. For this, we set $\alpha = 0$ and just
look at the upper tail (which is a reflection of the lower

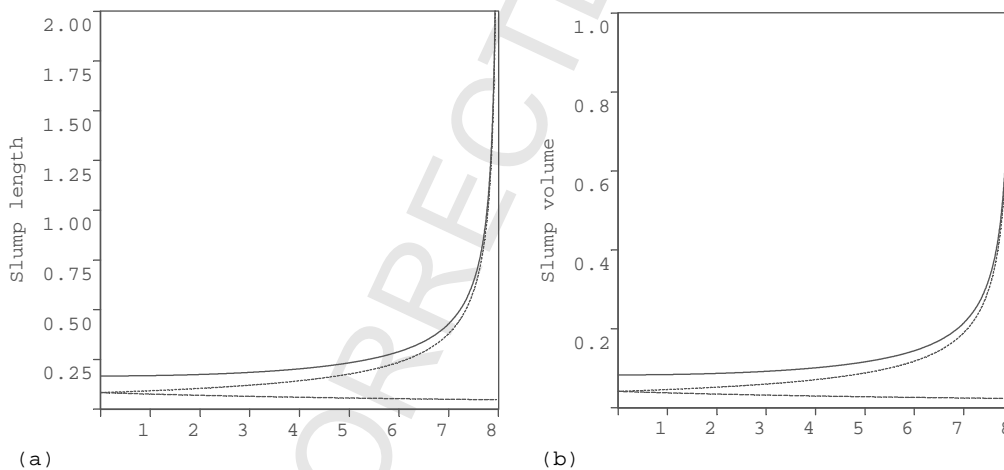


Fig. 5. Variation of slump length and slump volume with increasing inclination α : fixed parameters, $\tau_{c,Y} = \tau_{m,Y} = 1$: (a) upper tail slump length (dashed line), lower tail slump length (dashed line), and total slump length (solid line); (b) upper tail slump volume (dashed line), lower tail slump volume (dashed line), and total slump volume (solid line).

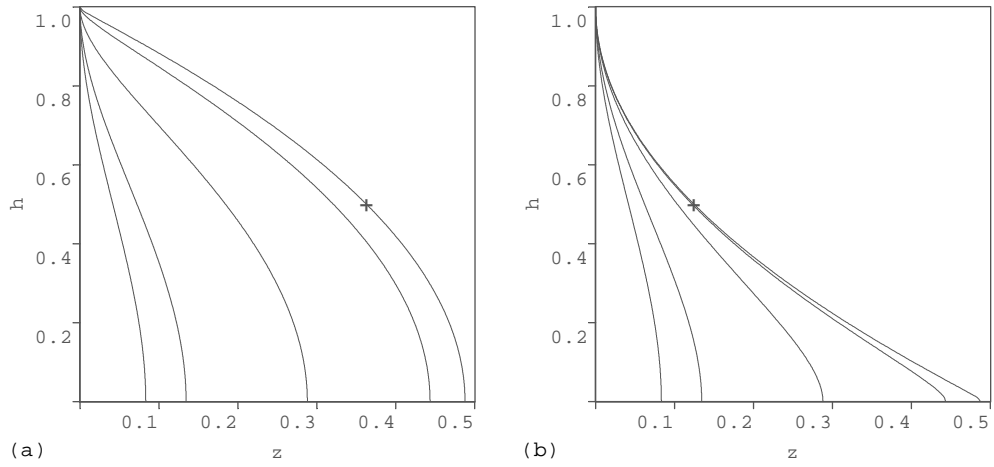


Fig. 6. Variation of slump shape with rheology in horizontal slot, $\alpha = 0$: (a) $\tau_{c,Y} = 1$, $\tau_{m,Y} = 1, 0.5, 0.1, 0.01, 0.001$, the curve $\tau_{m,Y} = 0.001$ is marked with a +; (b) $\tau_{m,Y} = 1$, $\tau_{c,Y} = 1, 0.5, 0.1, 0.01, 0.001$, the curve $\tau_{c,Y} = 0.001$ is marked with a +.

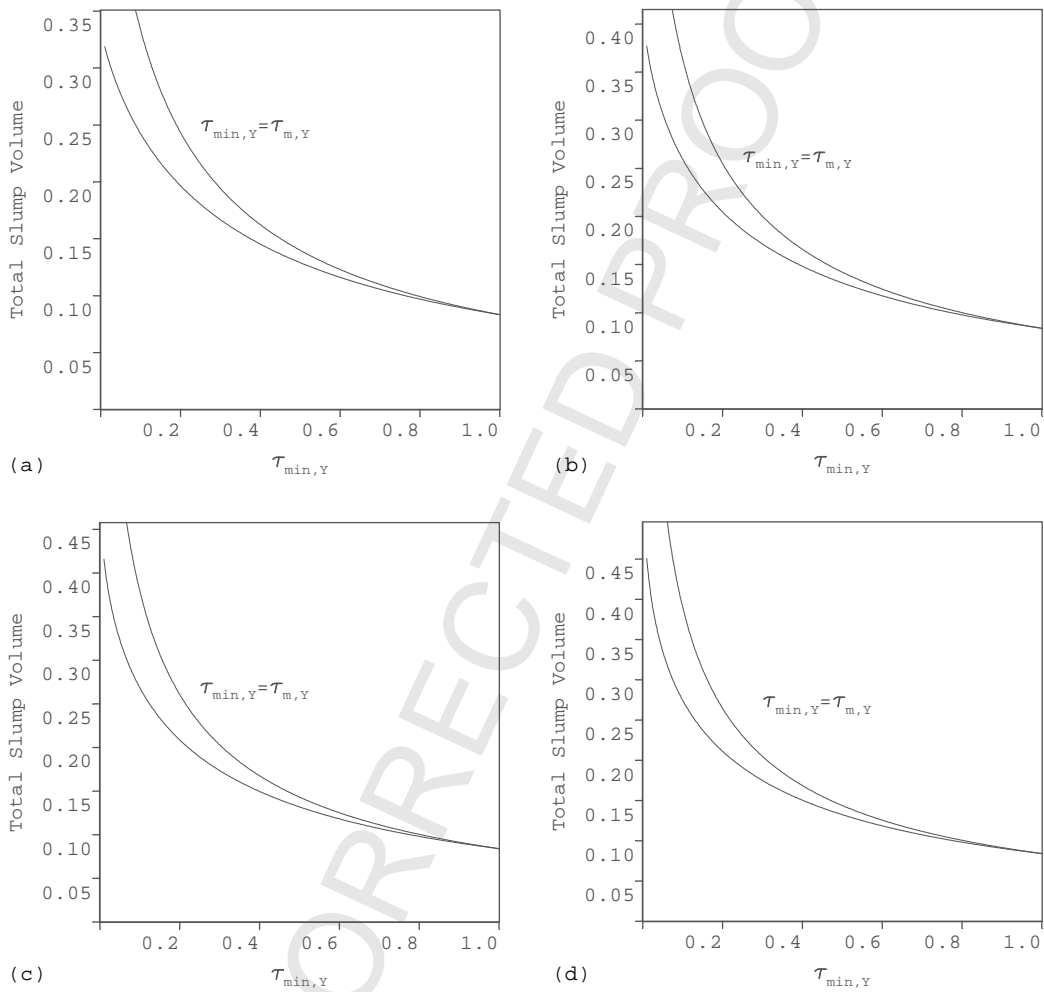


Fig. 7. Variations in total slump volume ($V_{total} = V_{upper} + V_{lower}$) with $\tau_{min,Y}$ for different α : (a) $\alpha = 0.0$; (b) $\alpha = 0.75$; (c) $\alpha = 0.9$; (d) $\alpha = 0.99$. The different curves are for $\tau_{min,Y} = \tau_{c,Y}$, $\tau_{m,Y} = 1$ (upper curve), and $\tau_{min,Y} = \tau_{m,Y}$, $\tau_{c,Y} = 1$ (lower curve).

465 tail). Fig. 6a shows the profile for $\tau_{c,Y} = 1$ and for de-
 466 creasing values of $\tau_{m,Y}$. When $\tau_{c,Y} = \tau_{m,Y}$, the profile is
 467 anti-symmetric about $h = 0.5$. Evidently, the slump length
 468 increases with decreasing $\tau_{m,Y}$, and the tail is seen to bulge
 469 outwards towards the bottom of the slot. Fig. 6b reverses
 470 the rheologies of Fig. 6a, and the results are seen to be a
 471 180° rotation from those in Fig. 6a. Interestingly, the slump
 472 volume is smaller in Fig. 6b than in Fig. 6a, i.e. effectively
 473 it is beneficial to have a mud yield stress holding back the
 474 cement, rather than the other way round.

475 To explore this asymmetry further, we have plotted in
 476 Fig. 7 the total slump volume against $\tau_{\min,Y}$ for the two
 477 cases: $\tau_{\min,Y} = \tau_{c,Y}$, $\tau_{m,Y} = 1$ (upper curve), and $\tau_{\min,Y} =$
 478 $\tau_{m,Y}$, $\tau_{c,Y} = 1$ (lower curve). We can see that the discrep-
 479 ancy between total volume for the different rheological combi-
 480 nations can be quite significant at small values of $\tau_{\min,Y}$.
 481 Whether or not this is (operationally or practically) signifi-
 482 cant depends on the ratio of tail volume to total plug volume.

483 **4. Slumping in a circular pipe**

484 We turn now to the more realistic situation of a slump-
 485 ing flow in a circular pipe. One approach to this prob-
 486 lem would be to find the solution (w, f) at each interface
 487 height h and then solve the transient problem for the in-
 488 terface motion. However, to find (w, f) is very time con-
 489 suming (in general requiring e.g. a two-dimensional elliptic
 490 finite element solver coupled with some form of iterative
 491 method, see e.g. [13]). Fortunately, conditions for the
 492 slumping flow to stop can be derived directly, as we show
 493 below.

494 Fig. 8 shows schematically the stratified interface geom-
 495 etry that we consider (by stratified, we mean that in each

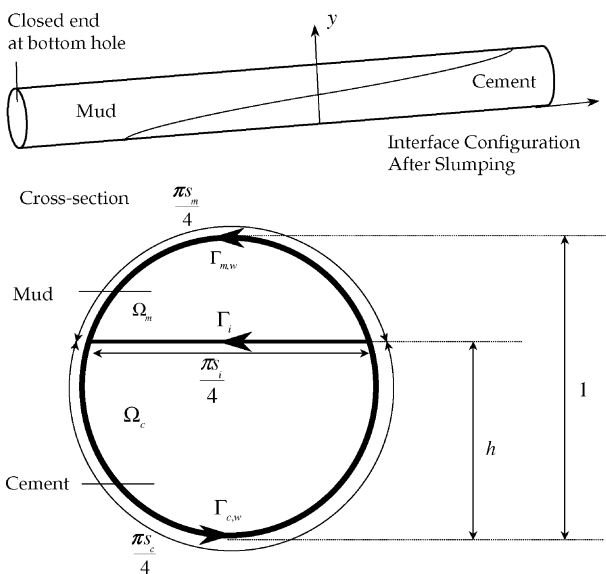


Fig. 8. Schematic diagram of the geometry for the stratified slumping flow, with the fluids separated by a linear interface.

cross-section the flow domains are separated by a linear in- 496
 terface, as illustrated). In place of the classical formulation 497
 (29) and (30), with Dirichlet boundary conditions and conti- 498
 nuity conditions across the interface, we consider the vari- 499
 ational formulation, which is derived in [10,13]. For arbit- 500
 rary $u, v \in H_0^1(\Omega)$ the following norms and functionals are 501
 defined: 502

$$a_k(u, v) = \int_{\Omega_k} \frac{\partial u}{\partial y} \frac{\partial v}{\partial y} + \frac{\partial u}{\partial z} \frac{\partial v}{\partial z} d\Omega, \quad k = c, m, \quad (51)$$

$$j_k(v) = \int_{\Omega_k} \left[\left(\frac{\partial v}{\partial y} \right)^2 + \left(\frac{\partial v}{\partial z} \right)^2 \right]^{1/2} d\Omega, \quad k = c, m, \quad (52)$$

$$a(u, v) = a_c(u, v) + m a_m(u, v), \quad (53)$$

$$j(v) = \tau_{c,Y} j_c(v) + \tau_{m,Y} j_m(v), \quad (54)$$

$$Q_k(v) = \int_{\Omega_k} v d\Omega, \quad k = c, m, \quad (55)$$

$$Q(v) = Q_c(v) + Q_m(v), \quad (56)$$

$$\|v\|_{L^1(\Omega)} = \int_{\Omega} |v| d\Omega, \quad (57)$$

$$\|v\|_{L^2(\Omega)}^2 = \int_{\Omega} v^2 d\Omega, \quad (58)$$

$$\|v\|_{H^1(\Omega)}^2 = \|v\|_{L^2(\Omega)}^2 + a_c(v, v) + a_m(v, v), \quad (59)$$

$$L(v) = fQ(v) - bQ_c(v). \quad (60)$$

The variational problem for the axial velocity w is to find 515
 $w \in H_0^1(\Omega)$ satisfying:² 516

$$a(w, v - w) + j(v) - j(w) \geq L(v - w), \quad (61)$$

$$\forall v \in H_0^1(\Omega), \quad w \in H_0^1(\Omega), \quad (61)$$

see also [32–34] for analogous single fluid problems. Note 520
 that if we wish also to satisfy the flow constraint (36) (i.e. to 521
 have $Q(w) = 0$), then the variational formulation is modi- 522
 fied: 523

$$a(w, v - w) + j(v) - j(w) \geq -bQ_c(v - w), \quad (62)$$

$$\forall v \in V_0(\Omega), \quad w \in V_0(\Omega), \quad (62)$$

where 527

$$V_0(\Omega) = \{v \in H_0^1(\Omega) : Q(v) = 0\}. \quad (62)$$

² Recall that $H_0^1(\Omega)$ is the space that results from completion of the 528
 space of functions $v \in C_0^\infty(\Omega)$ (i.e. smooth functions vanishing outside 529
 some compact subset of Ω), with respect to the norm: 530

$$\|v\| = \left[\int_{\Omega} v^2 + \left(\frac{\partial v}{\partial x_j} \right)^2 d\Omega \right]^{1/2}.$$

529 4.1. Limits for zero flow

530 We work within the above variational framework. As be-
 531 fore we first consider in detail the progression of the lower
 532 tail, stating later equivalent results for the upper tail. The
 533 same method can also be used to derive the limiting lengths
 534 for the slot flow before, and we include a sketch outline in
 535 Appendix A. Setting $v = 0$ and $v = 2w$ in (62) and combin-
 536 ing the two resulting inequalities, we see that the solution
 537 w of (62) satisfies:

$$538 \quad a(w, w) = -bQ_c(w) - j(w). \quad (63)$$

539 Note that for $w \in V_0$ we have that $Q_m(w) = -Q_c(w)$ and
 540 that $Q_m(w) > 0$ unless $w = 0$. Assuming now that $w \neq 0$,
 541 we derive conditions on b under which we must have $w = 0$.

$$542 \quad a(w, w) = Q_m(w) \left[b - \tau_{c,Y} \frac{j_c(w)}{-Q_c(w)} + \tau_{m,Y} \frac{j_m(w)}{Q_m(w)} \right],$$

$$544 \quad a(w, w) \leq Q_m(w) \left[b - \inf_{v \in V_0, v \neq 0} \left\{ \tau_{c,Y} \frac{j_c(v)}{-Q_c(v)} \right. \right. \\ \left. \left. + \tau_{m,Y} \frac{j_m(v)}{Q_m(v)} \right\} \right]. \quad (64)$$

546 Intuitively, the infimum in (64) is attained by maximising
 547 the flux through each Ω_k (positive in Ω_m , negative in Ω_c),
 548 whilst both minimising the area in which $|\nabla v| \neq 0$ and bal-
 549 ancing the fluxes so that $Q(v) = 0$. In Appendix A we show
 550 that the functional approach, stemming from (64), yields the
 551 same results as in (41) when applied to the simple slot flow
 552 model of Section 3. In [13] it is shown that the minimiser of
 553 this functional is the limit of a sequence of functions which
 554 are essentially constant in the interior of Ω_m and Ω_c , with
 555 thin boundary layers at the interface and walls, in which
 556 the continuity and no-slip conditions are satisfied. Geomet-
 557 rically, the infimum is thus related to various ratios of areas
 558 and perimeters, as is the general case for single fluid flows
 559 (see e.g. [35] for the single fluid case). In [13] the following
 560 analytical expression is derived:

$$562 \quad a(w, w) \leq Q_m(w) \left[b - \left\{ \tau_{c,Y} \frac{\beta_c(h)}{\beta_0(h)} + \tau_{m,Y} \frac{\beta_m(h)}{\beta_0(h)} \right. \right. \\ \left. \left. + \frac{\tau_{\min,Y}}{\beta_0(h)} \right\} \right], \quad (65)$$

564 where $\beta_0(h)$, $\beta_c(h)$ and $\beta_m(h)$ are defined by:

$$566 \quad \beta_0(h) \equiv \frac{\alpha_c \alpha_m}{s_i} = \frac{1}{16} \left[\frac{s_c s_m}{s_i} - (1 - 2h)^2 s_i \right. \\ \left. + (1 - 2h)(s_c - s_m) \right], \quad (66)$$

$$568 \quad \beta_m(h) \equiv \frac{\alpha_c s_m}{s_i} = \frac{1}{4} \left[\frac{s_c s_m}{s_i} - (1 - 2h) s_m \right], \quad (67)$$

$$569 \quad \beta_c(h) \equiv \frac{\alpha_m s_c}{s_i} = \frac{1}{4} \left[\frac{s_c s_m}{s_i} - (1 - 2h) s_c \right]. \quad (68)$$

The functions α_c , α_m , s_c , s_m and s_i , which depend only on
 h , are defined by:

$$\alpha_c(h) = 1 - \alpha_m(h) \\ \equiv \frac{1}{\pi} (\cos^{-1}(1 - 2h) - 2(1 - 2h)[h(1 - h)]^{0.5}), \quad (69)$$

$$s_c(h) = 4 - s_m(h) \equiv \frac{4}{\pi} \cos^{-1}(1 - 2h), \quad (70)$$

$$s_i(h) \equiv \frac{8}{\pi} [h(1 - h)]^{0.5}. \quad (71)$$

Geometrically, the functions α_c and α_m are the area fractions
 of Ω_c and Ω_m , respectively; s_c , s_m and s_i are the lengths of
 the boundaries $\Gamma_{c,w}$, $\Gamma_{m,w}$ and Γ_i (each divided through by
 $\pi/4$), as illustrated in Fig. 8. These functions are plotted in
 Fig. 9. To avoid difficulties in evaluating $\beta_0(h)$, $\beta_c(h)$ and
 $\beta_m(h)$ close to $h = 0$ and 1, the following expansions are
 used:

$$\frac{s_c s_m}{s_i}(h) \sim \frac{8}{\pi} \left[\frac{\pi - \cos^{-1}(1 - 2h)}{2\sqrt{1 - h}} \right] \\ \times \left[1 + \frac{h}{6} + \frac{3h^2}{20} + O(h^3) \right], \quad h \rightarrow 0, \quad (72)$$

$$\frac{s_c s_m}{s_i}(\delta) \sim \frac{8}{\pi} \left[\frac{\cos^{-1}(-1 + 2\delta)}{2\sqrt{1 - \delta}} \right] \left[1 + \frac{\delta}{6} + \frac{3\delta^2}{20} + O(\delta^3) \right], \\ \delta \rightarrow 0, \quad (73)$$

where $\delta = 1 - h > 0$. The functions $\beta_0(h)$, $\beta_c(h)$ and $\beta_m(h)$
 are plotted in Fig. 10.

From (65), since $Q_m(w) \geq 0$ and $a(w, w) = 0$ only if
 $w = 0$, we see that for each h we have $w = 0$ provided that:

$$b \leq \tau_{c,Y} \frac{\beta_c(h)}{\beta_0(h)} + \tau_{m,Y} \frac{\beta_m(h)}{\beta_0(h)} + \frac{\tau_{\min,Y}}{\beta_0(h)}. \quad (74)$$

Dividing through by b and defining $\tau_{k,Y}^* = \tau_{k,Y}/b$, $k =$
 c, m , we may take the maximum of the right-hand side of
 (74), with respect to $h \in [0, 1]$. Setting this maximum equal
 to 1 defines a curve in the $(\tau_{c,Y}^*, \tau_{m,Y}^*)$ plane, above which
 only trivial solutions are found. There is no easy analytical
 expression, but computation of the curve is straightforward
 (see [13]), and is plotted in Fig. 2b.

As with the slot flow of the previous section, for suffi-
 ciently small α (see below), the shape of the maximal lower
 slump tail is given by rearranging (74) and integrating:

$$\frac{d}{dh} z_{l,\max} = \frac{1}{\tau_{c,Y}(\beta_c(h)/\beta_0(h)) + \tau_{m,Y}(\beta_m(h)/\beta_0(h)) \\ + (\tau_{\min,Y}/\beta_0(h)) - \alpha}. \quad (75)$$

The maximal length which the lower tail can slump, L_{lower} ,
 is given by integrating (75) from $h = 0$ to 1, i.e.

$$L_{\text{lower}} = \int_0^1 \frac{1}{\tau_{c,Y}(\beta_c(h)/\beta_0(h)) + \tau_{m,Y}(\beta_m(h)/\beta_0(h)) \\ + (\tau_{\min,Y}/\beta_0(h)) - \alpha} dh \quad (76)$$

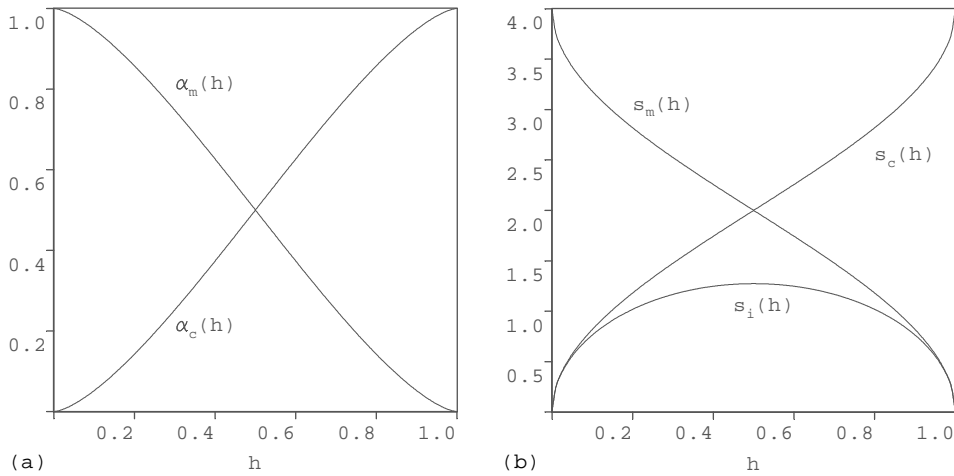


Fig. 9. The functions $\alpha_c(h)$, $\alpha_m(h)$, $s_c(h)$, $s_m(h)$ and $s_i(h)$.

613 and the total cement volume in the lower tail is

614
$$V_{\text{lower}} = \frac{\pi}{4} \int_0^1 s_i(h) [L_{\text{lower}} - z_{l,\text{max}}(h)] dh. \quad (77)$$

615 **4.1.1. Bounding α**

616 As with the slot flow we must bound $\alpha \leq \alpha_{\text{crit}}$, in order to
 617 ensure that the downwards slope of the pipe cannot promote
 618 a non-stationary flow on its own. The function α_{crit} depends
 619 only on $\tau_{\text{min},Y}$, and is computed from the marginal curve
 620 in Fig. 2b. If $\tau_{\text{min},Y} = 0$, then we see that we require $1/\alpha$,
 621 to exceed the end value of the curve in Fig. 2b. This value
 622 is given by ≈ 0.3043 , i.e. $\alpha \leq 3.2862 \dots$. At the other
 623 extreme, when $\tau_{\text{min},Y} = 1$ and the yield stresses are equal,
 624 the critical value is given by, $\alpha_{\text{crit}} = 8 + 16/\pi \approx 13.0929 \dots$
 625 In between these two values, computation is needed.

626 **4.1.2. Upper tail slump length**

627 An identical analysis may be carried out for the upper tail,
 628 giving the following expressions:

629
$$\frac{d}{dh} z_{u,\text{max}} = \frac{1}{\tau_{c,Y}(\beta_c(h)/\beta_0(h)) + \tau_{m,Y}(\beta_m(h)/\beta_0(h)) + (\tau_{\text{min},Y}/\beta_0(h)) + \alpha}, \quad (78)$$

630
$$L_{\text{upper}} = \int_0^1 \frac{1}{\tau_{c,Y}(\beta_c(h)/\beta_0(h)) + \tau_{m,Y}(\beta_m(h)/\beta_0(h)) + (\tau_{\text{min},Y}/\beta_0(h)) + \alpha} dh, \quad (79)$$

631
$$V_{\text{upper}} = \frac{\pi}{4} \int_0^1 s_i(h) [L_{\text{upper}} - z_{u,\text{max}}(h)] dh. \quad (80)$$

632 **4.2. Example results**

633 Analogous results to Figs. 5–7 are given in Figs. 11–13.
 634 Fig. 11 shows the effects of increasing α on the upper
 635 and lower slump tails. Compared to the slot flow
 636 there are two main differences. First, the inclinations re-

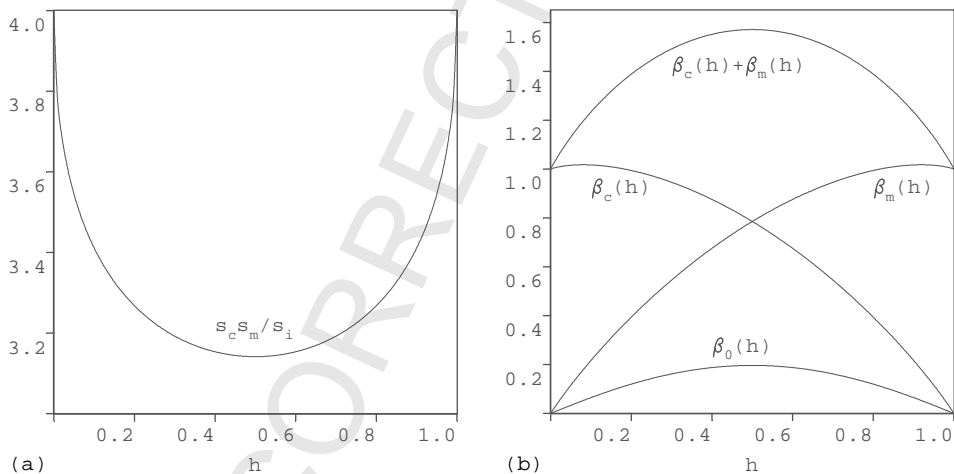


Fig. 10. The functions $(s_c s_m / s_i)(h)$, $\beta_0(h)$, $\beta_m(h)$, $\beta_c(h)$, $\beta_m(h) + \beta_c(h)$.

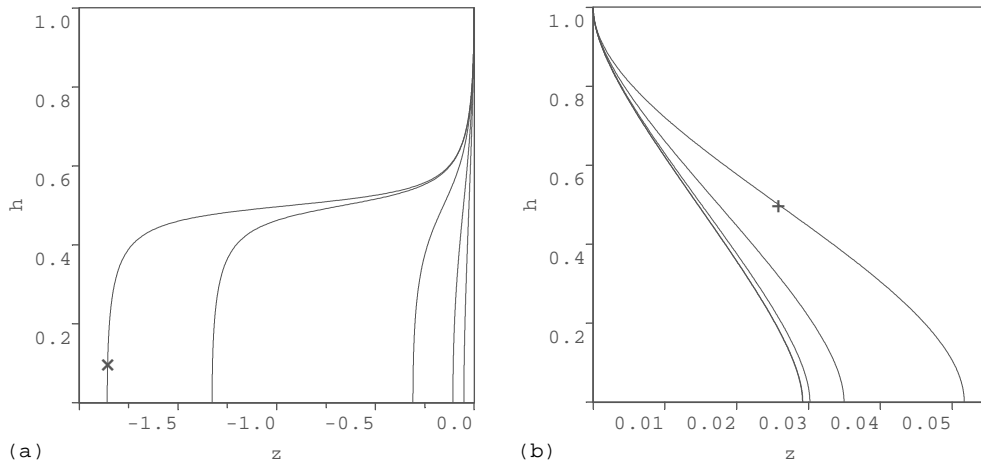


Fig. 11. Variation of upper and lower slump tail shape with increasing inclination, $\alpha = 0, 8, 12, 13, 13.0429 \dots$; here $\alpha_{crit} = 13.0929 \dots$: fixed parameters, $\tau_{c,Y} = \tau_{m,Y} = 1$: (a) lower slump tail increases with α , the curve $\alpha = 13.0429 \dots$ is marked with a \times ; (b) upper slump tail decreases with α , the curve $\alpha = 0$ is marked with a $+$.

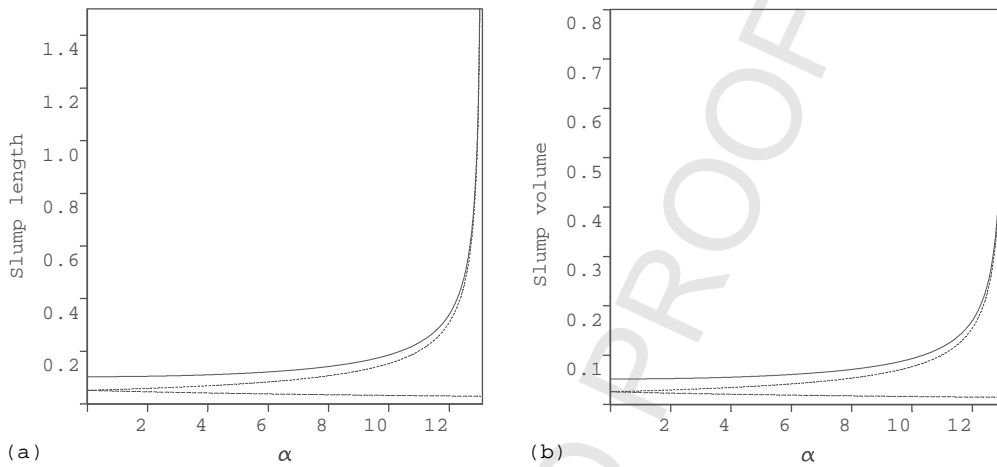


Fig. 12. Variation of slump length and slump volume with increasing inclination α : fixed parameters, $\tau_{c,Y} = \tau_{m,Y} = 1$: (a) upper tail slump length (dashed line), lower tail slump length (dashed line), and total slump length (solid line); (b) upper tail slump volume (dashed line), lower tail slump volume (dashed line), and total slump volume (solid line).

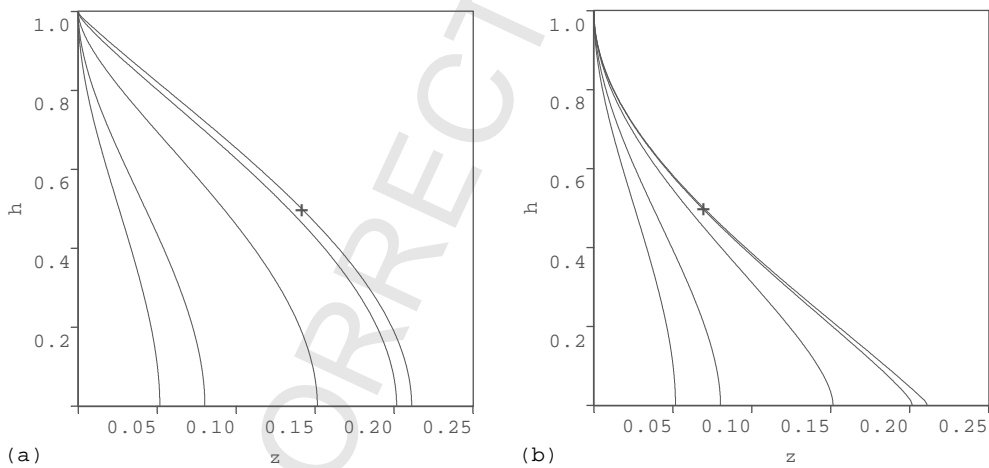


Fig. 13. Variation of slump shape with rheology in horizontal slot, $\alpha = 0$: (a) $\tau_{c,Y} = 1, \tau_{m,Y} = 1, 0.5, 0.1, 0.01, 0.001$, the curve $\tau_{m,Y} = 0.001$ is marked with a $+$; (b) $\tau_{m,Y} = 1, \tau_{c,Y} = 1, 0.5, 0.1, 0.01, 0.001$, the curve $\tau_{c,Y} = 0.001$ is marked with a $+$.

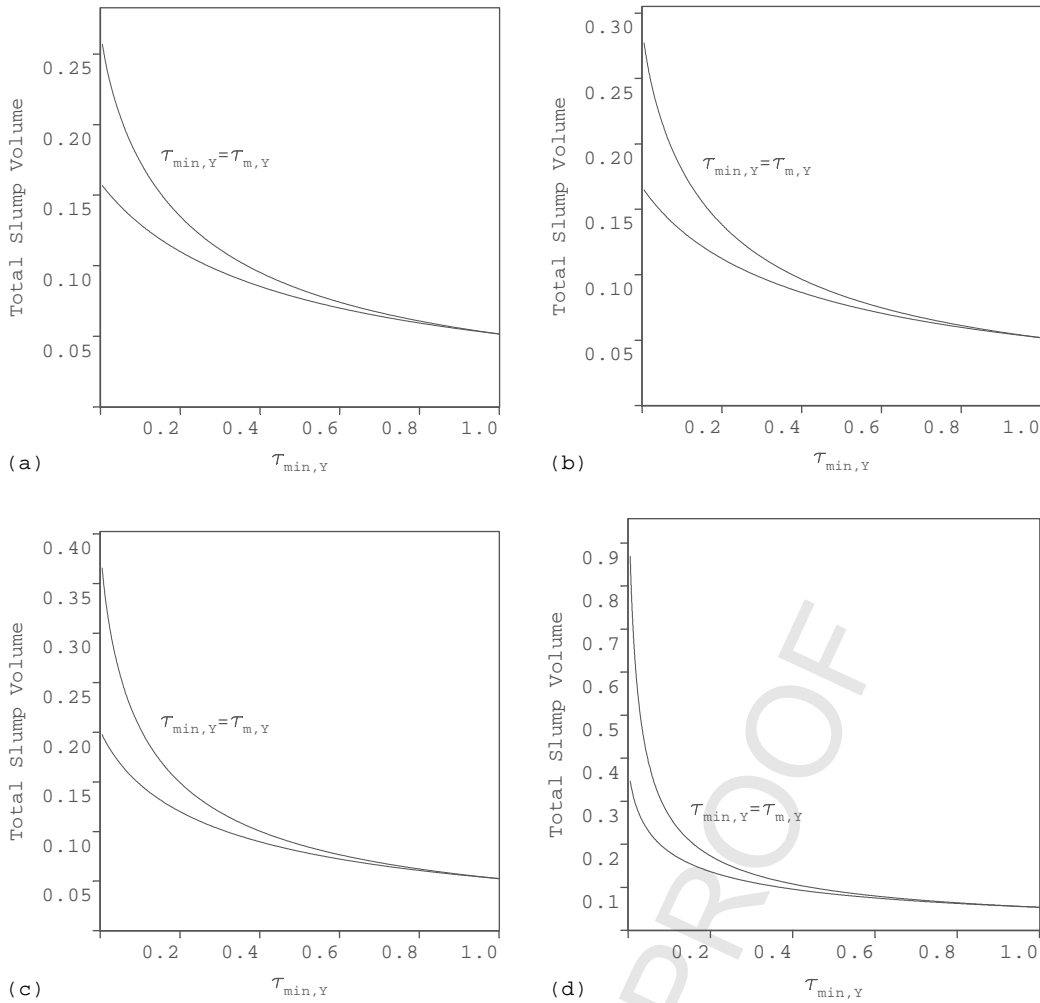


Fig. 14. Variations in total slump volume ($V_{total} = V_{upper} + V_{lower}$) with $\tau_{min,Y}$ for different α : (a) $\alpha = 0.0$; (b) $\alpha = 1$; (c) $\alpha = 2$; (d) $\alpha = 3$. The different curves are for $\tau_{min,Y} = \tau_{c,Y}$, $\tau_{m,Y} = 1$ (upper curve) and $\tau_{min,Y} = \tau_{m,Y}$, $\tau_{c,Y} = 1$ (lower curve).

640 quired in order to get a significant tail are much larger
 641 than for the slot. This is of course intuitive, since the
 642 walls of the pipe support the fluids. The critical value of
 643 α at which the flow runs away is $\alpha_{crit} = 8 + 16/\pi \approx$
 644 $13.0929\dots$, compared to $\alpha_{crit} = 8$ for the slot. The
 645 second difference is in interface profile with h . Com-
 646 pared to Fig. 5 we can see that the profiles in Fig. 11
 647 have strongly accentuated changes in h close to $h =$
 648 0.5 . This is of course the position at which it is easi-
 649 est for the interface to move in the pipe, since the side
 650 walls are distant. Fig. 12 is quite similar qualitatively to
 651 Fig. 6.

652 Comparing variations in slump shape with rheology (com-
 653 pare Fig. 13 with Fig. 7), we can see that the symmetry
 654 properties are preserved also for the pipe flow. Thus again,
 655 increasing the mud yield stress is more effective at reducing
 656 slump length than increasing the cement slurry yield stress.
 657 Otherwise the results are qualitatively similar. Overall, the
 658 slump lengths are significantly shorter for the pipe than for
 659 the slot.

4.3. Cement volumes required

660

For direct application to field design, the parameter of inter-
 661 est is the total volume of cement required, i.e. for an intact
 662 length of plug \hat{L}_{plug} , how much cement must be pumped.
 663 This quantity is given dimensionally as
 664

$$\hat{V}_{cement} = \frac{\pi \hat{D}^2 \hat{L}_{plug}}{4} + \frac{\hat{D}^3}{\delta} V_{total}, \tag{81} \quad 665$$

where δ is defined in (11) and V_{total} is the dimensionless
 666 total slump tail volume:
 667

$$V_{total} = V_{upper} + V_{lower}. \quad 668$$

In Fig. 14 we have plotted V_{total} as a function of $\tau_{min,Y}$ for
 669 a range of different inclinations.
 670

5. Discussion

671

In this paper we have derived conditions under which a
 672 slow slumping stratified flow in a near-horizontal well (or
 673

674 slot) will stop. The conditions are computable via fairly
675 straightforward quadrature and are thus ideally suited to ap-
676 plication in a field setting. Following the results in [9] for
677 the slot and [13] for the stratified interface in the pipe, the
678 expressions are in fact quite easy to derive, but this does not
679 negate their utility.

680 In terms of validation of our results, we may think of both
681 experimental and computational methods, the latter for the
682 transient problem. An experimental study appears feasible,
683 but also presents some significant challenges. First, exact
684 measurement of the yield stress of a model/laboratory fluid
685 is not straightforward and typically there is significant error.
686 Whereas measurement errors might have a less significant
687 effect on an experiment in which the flow behaviour of the
688 fluids is important, here it is only the yield stresses that
689 enter the final results. Second, we must note that our limiting
690 surfaces are upper bounds for the slump flow. For given
691 initial conditions, the flow may stop before this limiting
692 surface is attained. Initial interface and stress configurations
693 are hard to vary in an experimental setting, compared to a
694 numerical setting, so this is a restriction. Nevertheless, we
695 do here have both quantitative and qualitative predictions
696 that might be tested.

697 In so far as the transient problem goes, we see that it
698 amounts to solving an equation of form:

$$699 \quad h_t + \frac{\partial}{\partial z} Q_c(h, h_z) = 0. \quad (82)$$

700 Evidently, the behaviour of the interface depends wholly
701 on the initial conditions and on the flux function $Q_c(h, h_z)$
702 (effectively the flow rate through the cement). Numerical
703 solution of equations such as (82) has been carried out, for
704 example in [17,26], in both one and two dimensions, but in
705 these works the flux functions are simpler than here. It is
706 impossible to compute $Q_c(h, h_z)$ quickly for the stratified
707 interface in a circular pipe. This is, however, possible for
708 the slot flow problem. The static problems that we have
709 considered are qualitatively similar and we might expect
710 similar behaviours also for the transient problems.

711 In general, we expect that $Q_c(h, h_z) \rightarrow 0$ for both small
712 and large values of $h \in [0, 1]$, at any fixed h_z , and thus we
713 have two points of degeneracy of (82). We are still study-
714 ing suitable methods for accurate computation of (82) and
715 intend to use these to study both the approach to the static
716 (maximal) solutions above and the flow when α_{crit} is ex-
717 ceeded. Although in two-dimensional free-surface flows, as
718 in [26], the final stopping surface can vary significantly with
719 the initial condition, here the motions are more restricted and
720 the maximal static surfaces computed should act as upper
721 bounds on the slump flow for any initial condition starting
722 below the surfaces. This is of course not proven.

723 If we freeze the h_z -dependency of $Q_c(h, h_z)$, by setting
724 $b = \text{constant}$, we recover a hyperbolic problem, which has
725 been studied at length in [11]. For the hyperbolic problem,
726 when non-zero flow occurs, it is known that the interface
727 transforms quickly into two shocks that travel up and down

728 the duct close to $h = 0$ and 1, stretching the interface be-
729 tween them. Intuitively, we expect the introduction of the
730 h_z -dependency to modify this behaviour slightly. For $\alpha >$
731 α_{crit} , we would still expect travelling waves, but the shocks
732 will be smoothed by the interface gradient. For $\alpha < \alpha_{\text{crit}}$ we
733 would intuitively expect that solutions to (82) will spread
734 diffusively towards the limiting interface shapes at which
735 motion stops. Again we cannot prove this, but we can at
736 least establish the diffusive nature of (82). Differentiating,
737 we see that (82) is equivalent to

$$738 \quad h_t + \frac{\partial Q_c}{\partial h} h_z = - \frac{\partial Q_c}{\partial h_z} h_{zz}. \quad (83)$$

739 We consider (h, h_z) such that $Q_c \neq 0$ and see that (82) is
740 diffusive in nature if

$$741 \quad \frac{\partial Q_c}{\partial h_z} < 0.$$

742 This is equivalent to showing that Q_c decreases with b ,
743 which we are able to demonstrate as follows. Consider two
744 values, $b_1 < b_2$, and the two solutions, w_1 and w_2 , to (62)
745 for these respective values of b . Clearly, in the variational
746 setting, w_1 is a test function for w_2 and vice versa. Sub-
747 stituting into (62) and subtracting the two inequalities, we
748 derive straightforwardly that

$$749 \quad 0 \leq a(w_1 - w_2, w_1 - w_2) \\ 750 \quad \leq -(b_1 - b_2)[Q_c(w_1) - Q_c(w_2)] \quad (84)$$

751 and hence Q_c decreases with b . Actual solution of the
752 non-linear parabolic problem (82) is the subject of ongoing
753 work. 754

755 Acknowledgements

756 The research contribution of IF was supported by NSERC
757 Canada. GN was funded by a commonwealth research fel-
758 lowship. Both authors express their appreciation for their fi-
759 nancial support. This research was initiated and largely car-
760 ried out in Oxford (which is somewhat equidistant between
761 Vancouver and Buea), during research visits to the Oxford
762 Centre for Industrial and Applied Mathematics (IF) and to
763 the Oxford Centre for Mathematical Biology (GN). We thank
764 S.D. Howison and P.K. Maini, respectively, for their kind in-
765 vitations and for the hospitality of their respective institutes.

766 Appendix A. Illustration of the functional analytic 767 approach

768 We here demonstrate that the functional analytic approach
769 does in fact produce the same results as the more mechanical
770 approach from [9]. We reconsider the slot flow model of
771 Section 3 in the functional context of Section 4, and will
772 derive condition (41). We adopt an informal and intuitive
773 manner, although rigorous proof could be constructed.

774 Assuming $w \neq 0$, we have from (64) the following in-
 775 equality:

$$777 \quad a(w, w) \leq Q_m(w) \left[b - \inf_{v \in V_0, v \neq 0} \left\{ \tau_{c,Y} \frac{j_c(v)}{-Q_c(v)} \right. \right. \\ 778 \quad \left. \left. + \tau_{m,Y} \frac{j_m(v)}{Q_m(v)} \right\} \right]. \quad (\text{A.1})$$

779 We define $F(h, \tau_{c,Y}, \tau_{m,Y})$ as

$$781 \quad F(h, \tau_{c,Y}, \tau_{m,Y}) = \inf_{v \in V_0, v \neq 0} \left\{ \tau_{c,Y} \frac{j_c(v)}{-Q_c(v)} + \tau_{m,Y} \frac{j_m(v)}{Q_m(v)} \right\} \\ 782 \quad (\text{A.2})$$

783 and will evaluate $F(h, \tau_{c,Y}, \tau_{m,Y})$. For the slot flow model,
 784 the various functionals on the right-hand side of (A.2) take
 785 the following forms:

$$787 \quad F(h, \tau_{c,Y}, \tau_{m,Y}) \\ 788 \quad = \inf_{v \in V_0, v \neq 0} \left\{ \tau_{c,Y} \frac{\int_0^h |v'(y)| dy}{-\int_0^h v(y) dy} + \tau_{m,Y} \frac{\int_h^1 |v'(y)| dy}{\int_h^1 v(y) dy} \right\}.$$

789 It is evident that this entire functional can be scaled. For a
 790 test solution $v \in V_0$, by definition of V_0 , we have that:

$$791 \quad -\int_0^h v(y) dy = \int_h^1 v(y) dy,$$

792 (i.e. there is no net flux), and if $v \neq 0$, we may divide by
 793 the flow rate in either layer

$$795 \quad F(h, \tau_{c,Y}, \tau_{m,Y}) \\ 796 \quad = \inf_{v \in V_0, v \neq 0, \int_0^1 v(y) dy = 1} \left\{ \tau_{c,Y} j_c(v) + \tau_{m,Y} j_m(v) \right\}, \\ 797 \quad (\text{A.3})$$

798 taking the flow constraint into the test space. Now consider
 799 the type of function that will approximately minimise the
 800 functional on the right-hand side of (A.3). Consider first the
 801 interval $(0, h)$. The function $v(y)$ should obviously minimise
 802 $v'(y)$, which is best achieved if $v(y)$ is constant. The con-
 803 straint that

$$804 \quad 1 = -\int_0^h v(y) dy$$

805 suggests that $v(y) = -1/h$, will be a good choice. Similarly,
 806 on the interval $(h, 1)$, we can see that $v(y) = 1/(1-h)$, will
 807 be a good choice. However, this piecewise constant function
 808 does not satisfy the boundary conditions at $y = 0$ and 1 , nor
 809 does it satisfy continuity conditions at $y = h$. Therefore, we
 810 modify the function slightly, to say $v_\epsilon(y)$, by the addition
 811 of thin layers, of width $\epsilon \ll 1$, close to the interface and
 812 walls in which $v_\epsilon(y)$ varies linearly between the constant
 813 values and boundary values. The function $v_\epsilon(y)$ is shown
 814 schematically in Fig. 15.

815 We may infer that the function $v_\epsilon(y)$ is close to the min-
 816 imiser of (A.3), and that $v_\epsilon(y)$ will adopt constant values:

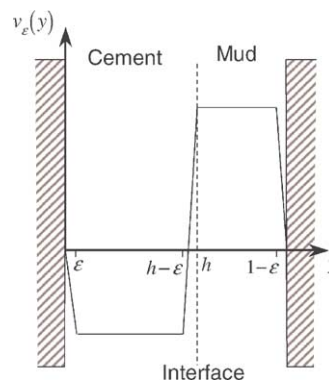


Fig. 15. Schematic diagram of the near-optimal function $v_\epsilon(y)$, assuming $\tau_{c,Y} < \tau_{m,Y}$.

817 $v_\epsilon(y) \sim -1/h + O(\epsilon)$ and $v_\epsilon(y) \sim 1/(1-h) + O(\epsilon)$, on
 818 the bulk of the two intervals, $(0, h)$ and $(h, 1)$, respectively.
 819 By inspection of (A.3), we see that by placing the transition
 820 layer at the interface within the fluid with the smaller yield
 821 stress (i.e. Fig. 15 assumes that $\tau_{c,Y} < \tau_{m,Y}$), the functional
 822 in (A.3) is minimised. We have therefore that

$$824 \quad \tau_{c,Y} j_c(v_\epsilon) + \tau_{m,Y} j_m(v_\epsilon) \\ 825 \quad \sim \frac{\tau_{c,Y}}{h} + \frac{\tau_{m,Y}}{1-h} + \tau_{\min,Y} \left[\frac{1}{1-h} + \frac{1}{h} \right] + O(\epsilon).$$

826 If we now consider that the infimum defining $F(h, \tau_{c,Y}, \tau_{m,Y})$
 827 is attained by a sequence of functions $v_\epsilon(y)$, for which
 828 $\epsilon \rightarrow 0$, we have that

$$830 \quad F(h, \tau_{c,Y}, \tau_{m,Y}) = \frac{\tau_{c,Y}}{h} + \frac{\tau_{m,Y}}{1-h} + \tau_{\min,Y} \left[\frac{1}{1-h} + \frac{1}{h} \right] \\ 831 \quad (\text{A.4})$$

and from (A.1) it follows that $w = 0$ if

$$833 \quad b \leq \frac{\tau_{c,Y}}{h} + \frac{\tau_{m,Y}}{1-h} + \tau_{\min,Y} \left[\frac{1}{1-h} + \frac{1}{h} \right], \quad (\text{A.5})$$

834 which is condition (41), from Section 3.

835 Finally, we may note that since $|v'_\epsilon(y)|$ is integrated with
 836 respect to y , it is not particularly important how $v_\epsilon(y)$
 837 varies between the constant values that it assumes, i.e.
 838 only the end values are important. If we consider how the
 839 actual solution must look like, in the limit of zero flow,
 840 we see that $w(y)$ will have large unyielded plug regions
 841 bounded by thin yielded layers close to the walls and inter-
 842 face. Indeed, $w(y)$ is also most likely to yield at the
 843 interface in the fluid with the smallest yield stress. Thus,
 844 $w(y)$ closely resembles $v_\epsilon(y)$ (apart from an insignificant
 845 scaling and in having parabolic yielded velocity profile).
 846 Thus, we may infer that as we approach the yield lim-
 847 its, the velocity solution $w(y)$ approaches a minimiser of
 848 (A.2), and hence we suppose that the yield limit above
 849 is sharp.

850 **References**

- 851 [1] D.K. Smith, Cementing, SPE monograph series, Society of Petroleum
852 Engineers, 1987.
- 853 [2] E.B. Nelson, Well Cementing, Schlumberger Educational Services,
854 1990.
- 855 [3] R.M. Beirute, Flow behaviour of an unset cement plug in place,
856 Society of Petroleum Engineers Paper Number SPE 7589, 1978.
- 857 [4] D.L. Bour, D.L. Sutton, P.G. Creel, Development of effective methods
858 for placing competent cement plugs, Society of Petroleum Engineers
859 Paper Number SPE 15008, 1986.
- 860 [5] D.G. Calvert, J.F. Heathman, J.E. Griffith, Plug cementing: horizontal
861 to vertical conditions, Society of Petroleum Engineers Paper Number
862 SPE 30514, 1995.
- 863 [6] K. Harestad, T.P. Herigstad, A. Torsvoll, N.E. Nødland, A. Saasen,
864 Optimization of balanced-plug cementing, Society of Petroleum En-
865 gineers Paper Number SPE 33084, 1997.
- 866 [7] R.C. Smith, R.M. Beirute, G.B. Holman, Improved method of setting
867 successful whipstock cement plugs, Society of Petroleum Engineers
868 Paper Number SPE 11415, 1983.
- 869 [8] J.P. Crawshaw, I.A. Frigaard, Cement plugs: stability and failure by a
870 buoyancy-driven mechanism, Society of Petroleum Engineers Paper
871 Number SPE 56959, 1999.
- 872 [9] I.A. Frigaard, Stratified exchange flows of two Bingham fluids in an
873 inclined slot, *J. Non-Newtonian Fluid Mech.* 78 (1998) 61–87.
- 874 [10] I.A. Frigaard, O. Scherzer, Uniaxial Exchange Flows of Two Bingham
875 Fluids in a Cylindrical Duct, *IMA J. Appl. Math.* 61 (1998) 237–
876 266.
- 877 [11] H. Fenie, I.A. Frigaard, Preventing buoyancy driven flows of two
878 Bingham fluids in a closed pipe: fluid rheology design for oil-
879 field plug cementing, *Math. Comput. Modell.* 30 (7–8) (1999) 71–
880 91.
- 881 [12] I.A. Frigaard, J. Crawshaw, Preventing buoyancy driven flows of two
882 Bingham fluids in a closed pipe; fluid rheology design for oilfield
883 plug cementing, *J. Engng. Math.* 36 (1999) 327–348.
- 884 [13] I.A. Frigaard, O. Scherzer, The effects of yield stress variation on
885 uniaxial exchange flows of two Bingham fluids in a pipe, *SIAM J.*
886 *Appl. Math.* 60 (6) (2000) 1950–1976.
- 887 [14] R.W. Griffiths, J.H. Fink, Solidifying Bingham extrusions: a model
888 for the growth of silicic lava domes, *J. Fluid Mech.* 347 (1997)
889 13–36.
- 890 [15] R.W. Griffiths, The dynamics of lava flows, *Annu. Rev. Fluid Mech.*
891 32 (2000) 477–518.
- 892 [16] N.J. Balmforth, A.S. Burbidge, R.V. Craster, J. Salzig, A. Shen,
893 Visco-plastic models of isothermal lava domes, *J. Fluid Mech.* 403
894 (2000) 37–65.
- [17] N.J. Balmforth, R.V. Craster, Dynamics of cooling domes of
visco-plastic fluid, *J. Fluid Mech.* 422 (2000) 225–248. 895
- [18] N.J. Balmforth, A.S. Burbidge, R.V. Craster, Shallow lava theory,
in: N.J. Balmforth, A. Provenzale (Eds.), *Geomorphological Fluid*
Mechanics, Springer-Verlag, Berlin, 2001, pp. 164–187. 896
897
898
899
- [19] P. Coussot, *Mud Flow Rheology and Dynamics*, IAHR/AIRH Mono-
graph, 1997. 900
901
- [20] P. Coussot, S. Proust, Slow, unconfined spreading of a mud flow, *J.*
Geophys. Res. 101 (1996) 25217–25229. 902
903
- [21] P. Coussot, S. Proust, C. Ancey, Rheological interpretation of deposits
of yield stress fluids, *J. Non-Newtonian Fluid Mech.* 66 (1996) 55–
70. 904
905
906
- [22] X. Huang, M.H. Garcia, A Herschel–Bulkley model for mud flow
down a slope, *J. Fluid Mech.* 374 (1998) 305–333. 907
908
- [23] S.D.R. Wilson, S.L. Burgess, The steady, spreading flow of a rivulet
of mud, *J. Non-Newtonian Fluid Mech.* 79 (1998) 77–85. 909
910
- [24] K.F. Liu, C.C. Mei, Slow spreading of a sheet of Bingham fluid on
an inclined plane, *J. Fluid Mech.* 207 (1989) 505–529. 911
912
- [25] K.F. Liu, C.C. Mei, Approximate equations for the slow spreading of
a thin sheet of Bingham plastic fluid, *Phys. Fluids A* 2 (1990) 30–36. 913
914
- [26] C.C. Mei, M. Yuhi, Slow flow of a Bingham fluid in a shallow
channel of finite width, *J. Fluid Mech.* 431 (2001) 135–159. 915
916
- [27] A.B. Ross, S.K. Wilson, B.R. Duffy, Thin-film flow of a viscoplastic
material round a large horizontal stationary or rotating cylinder, *J.*
Fluid Mech. 430 (2001) 309–333. 917
918
919
- [28] S.K. Wilson, B.R. Duffy, A.B. Ross, On the gravity-driven draining
of a rivulet of viscoplastic material down a slowly varying substrate,
Phys. Fluids 14 (2002) 555–571. 920
921
922
- [29] J.M. Piau, Flow of a yield stress fluid in a long domain. Application
to flow on an inclined plane, *J. Rheol.* 40 (1996) 711–723. 923
924
- [30] N.J. Balmforth, R.V. Craster, A consistent thin-layer theory for Bing-
ham plastics, *J. Non-Newtonian Fluid Mech.* 84 (1999) 65–81. 925
926
- [31] N. Pashias, D.V. Boger, J. Summers, D.J. Glenister, A fifty cent
rheometer for yield stress measurement, *J. Rheol.* 40 (1996) 1179–
1189. 927
928
929
- [32] G. Duvaut, J.L. Lions, *Inequalities in Mechanics and Physics*, vol.
219, Springer-Verlag, Berlin, 1976, pp. 279–327. 930
931
- [33] R. Glowinski, J.L. Lions, R. Tremolieres, *Numerical Analysis of*
Variational Inequalities, North-Holland, Amsterdam, 1981; translated
from the French version: *Analyse numérique des inéquations varia-*
tionnelles, vols. 1 and 2, Dunod, Paris, 1976. 932
933
934
935
- [34] R. Glowinski, *Numerical Methods for Nonlinear Variational Prob-*
lems, Springer-Verlag, Berlin, 1983. 936
937
- [35] P.P. Mossolov, V.P. Miasnikov, Variational methods in the theory of
the fluidity of a viscous plastic medium, *J. Mech. Appl. Math.* 29 (3)
(1965) 468–492. 938
939
940